Data publication: Virtual experiments for steel fiber reinforced high performance concrete (HPC)

Mangesh Pise, Dominik Brands and Jörg Schröder

Institute of Mechanics, Faculty of Engineering/ Department Civil Engineering, University of Duisburg-Essen, Universitätsstr. 12, 45141 Essen, Germany
e-mail: mangesh.pise@uni-due.de, dominik.brands@uni-due.de, j.schroeder@uni-due.de
https://doi.org/10.5281/zenodo.10986296

1. Ellipsoidal RVE for fiber-reinforced HPC

The ellipsoidal RVE containing a single steel fiber is discretized using linear hexahedral element, as shown in Fig. 1. The discretization is done such that periodic boundary conditions can be applied on RVE.

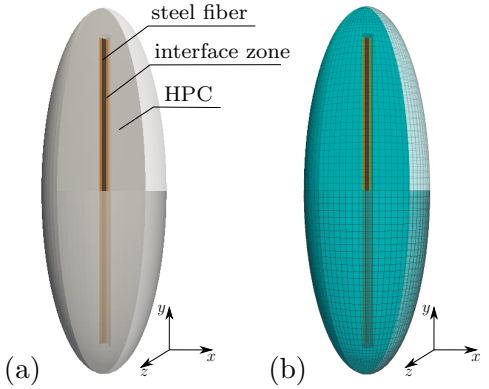

Figure 1: The representative volume element (RVE) (a) components of an ellipsodal RVE and (b) a discretized ellipsodal RVE used in the simulations, taken from Pise et al. [2021; 2022; submitted 2024].

2. Virtual experiments I-V

The virtual experiments with an attached ellipsodal RVE at the material point considering different types of loading conditions are shown in Fig. 2i-v, as given below.

(i) Virtual experiment I - uniaxial tensile test with vanishing transverse stresses.

(ii) Virtual experiment II - uniaxial tensile test transversely constrained.

(iii) Virtual experiment III - uniaxial tensile test with transverse compression.

(iv) Virtual experiment IV - uniaxial tensile test in transverse direction.

(v) Virtual experiment V - shear test.

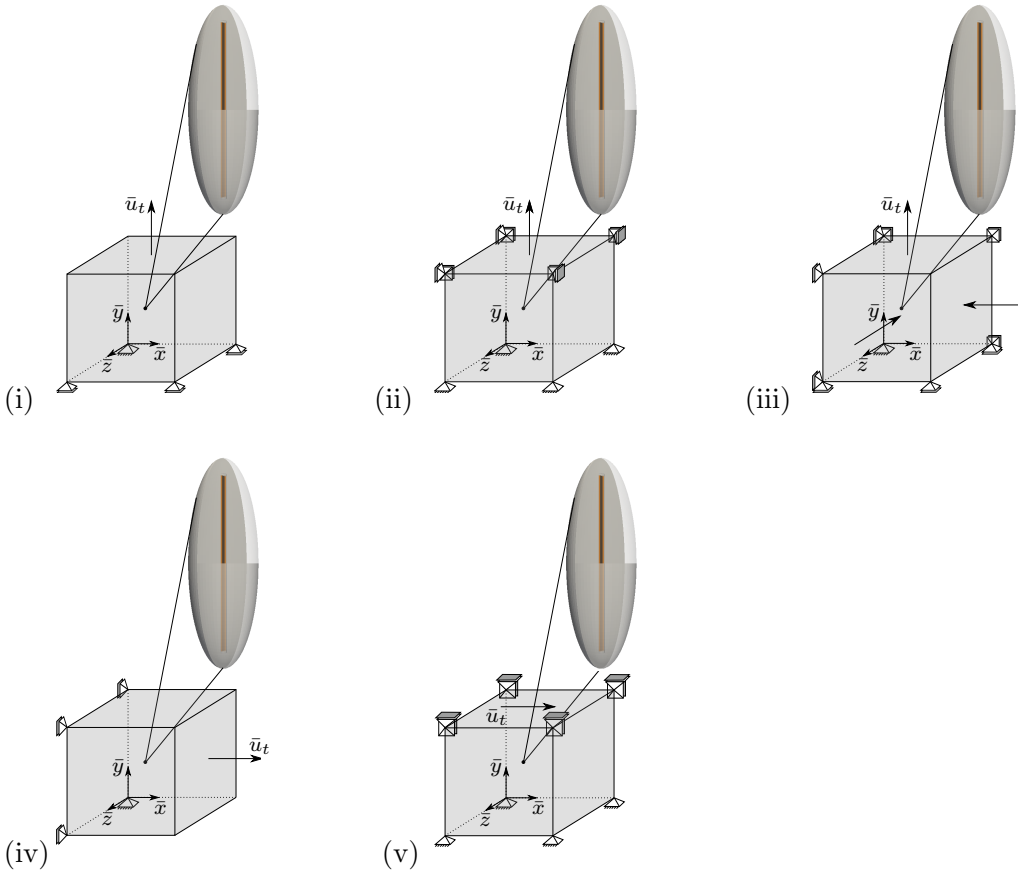

Figure 2: Virtual experiments I-V considering (i-v) different types of loading conditions, respectively, adopted from Pise et al. [2022; submitted 2024].

3. Application of loading conditions on an ellipsoid RVE

The boundary conditions are applied on the RVE by setting the value of strain components of using the macroscopic strain tensors $\bar{\boldsymbol{\varepsilon}}$ as shown Fig. 3i-v respectively from virtual experiments I-V.

$$\bar{\boldsymbol{\varepsilon}} = \begin{bmatrix} \bar{\varepsilon}^*_{11} & 0 & 0 \\ 0 & \bar{\varepsilon}_{22} & 0 \\ 0 & 0 & \bar{\varepsilon}^*_{33} \end{bmatrix} \quad \text{(i)} \qquad \bar{\boldsymbol{\varepsilon}} = \begin{bmatrix} 0 & 0 & 0 \\ 0 & \bar{\varepsilon}_{22} & 0 \\ 0 & 0 & 0 \end{bmatrix} \quad \text{(ii)} \qquad \bar{\boldsymbol{\varepsilon}} = \begin{bmatrix} -2\nu\bar{\varepsilon}_{22} & 0 & 0 \\ 0 & \bar{\varepsilon}_{22} & 0 \\ 0 & 0 & -2\nu\bar{\varepsilon}_{22} \end{bmatrix} \quad \text{(iii)}$$

$$\bar{\boldsymbol{\varepsilon}} = \begin{bmatrix} \bar{\varepsilon}_{11} & 0 & 0 \\ 0 & \bar{\varepsilon}^*_{22} & 0 \\ 0 & 0 & \bar{\varepsilon}^*_{33} \end{bmatrix} \quad \text{(iv)} \qquad \bar{\boldsymbol{\varepsilon}} = \begin{bmatrix} 0 & \bar{\varepsilon}_{12} & 0 \\ \bar{\varepsilon}_{12} & 0 & 0 \\ 0 & 0 & 0 \end{bmatrix} \quad \text{(v)}$$

Figure 3: Macroscopic strain tensors $\bar{\boldsymbol{\varepsilon}}$ applied to RVE according to the considered loading condition for virtual experiment I-V, taken from Pise et al. [2021; 2022; submitted 2024].

*Note, that due to the stress-free-requirement on the associated direction, these strain values are iteratively determined to achieve vanishing transverse stress condition.

4. Material parameters

Material parameters and mechanical properties of steel fiber and HPC used for the numerical solution are listed in Table 1.

Table 1: Material parameters and mechanical properties of steel fiber and HPC, cf. Gebuhr et al. [2019], Pise et al. [2021], Storm et al. [2021], Pise et al. [submitted 2024].

	E	ν	f_t	f_c	$\psi_\mathrm{t}^\mathrm{c}$	$\psi_\mathrm{c}^\mathrm{c}$	y_0	β_p	h	m	ζ
	GPa	–	MPa	MPa	MPa	MPa	–	–	mm	–	–
Steel	210	0.3	1150	–	0.4	0.4	660	0	130	0.6	0.5
Interface	39.976	0.192	–	–	2e-4	2e-4	6.263	0	0	0.3	0.5
HPC	39.976	0.192	5.7	112	4.2e-4	0.12	6.263	0.5218	2000	0.6	0.5

- The mechanical properties of steel fibers 3D 55/60 are provided by the supplier Bekaert GmbH.
- The measured mechanical properties of HPC in the experiment are taken from Gebuhr et al. [2019].

5. Numerical results

Comparison of macroscopic stress-strain characteristic using the ellipsoidal RVE of pure and reinforced HPC without perturbation and with 20% perturbation are shown exemplary for virtual experiment I in Fig.4.

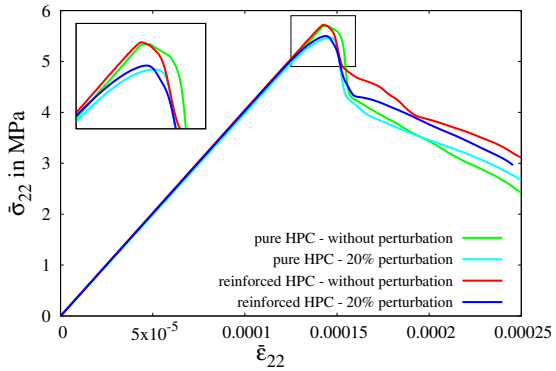

Figure 4: Virtual experiment I: comparison of macroscopic stress-strain characteristic using pure and reinforced ellipsoidal RVE without perturbation and with 20% perturbation, taken from Pise et al. [submitted 2024].

Further diagram of virtual experiment II-V can be derived from data sets, see section 7.

6. Solution scheme

- The steps for strain loading $\Delta\varepsilon = 5 \times 10^{-7}$ for virtual experiment I, II, IV and and $\Delta\varepsilon = 1 \times 10^{-6}$ for virtual experiment III and V are used along with the staggered solution scheme, cf. Ambati et al. [2015] and Seleš et al. [2019].

- The macro-mechanical model presented in Pise et al. [submitted 2024] is implemented in the framework of the Finite Element Method using the finite element analysis program FEAP (version 8.2) (A Finite Element Analysis Program by R.L. Taylor, UC, Berkeley), see Taylor [2008].

7. Appendix

The following files are included within this data publication:

1. Nodal coordinates for an ellipsodal RVE: *Feapnodes.dat*
2. Element connectivity for an ellipsodal RVE: *Feapelements.dat*
3. Nodal coordinates for the fixed nodes for an ellipsodal RVE: *Fixednodes.dat*
4. Nodal coordinates for the linked nodes for an ellipsodal RVE: *Linkednodes.dat*
5. Load-displacement plots for virtual experiments I-V in the separate folders:
   i. ellipsoid for pure concrete without fiber:
   plot-ellipsoid-pure-concrete.dat
   ii. ellipsoid for pure concrete with 20% of perturbation:
   plot-ellipsoid-pure-concrete-0.2.dat
   iii. ellipsoid for reinforced concrete with fiber:
   plot-ellipsoid-reinforced-concrete.dat
   iv. ellipsoid for reinforced concrete with 20% of perturbation:
   plot-ellipsoid-reinforced-concrete-0.2.dat

References

M. Ambati, T. Gerasimov, and L. De Lorenzis. Phase-field modeling of ductile fracture. *Computational Mechanics*, 55(5):1017–1040, 2015.

G. Gebuhr, M. Pise, M. Sarhil, S. Anders, D. Brands, and J. Schröder. Analysis and evaluation of the pull-out behavior of hooked steel fibers embedded in high and ultra-high performance concrete for calibration of numerical models. *Structural Concrete*, 20 (4):1254–1264, 2019.

M. Pise, D. Brands, J. Schröder, G. Gebuhr, and S. Anders. Macroscopic model for steel fiber reinforced high performance concrete based on unit cell calculations. *Proceedings in Applied Mathematics and Mechanics*, 21(1):e202100180, 2021.

M. Pise, D. Brands, J. Schröder, G. Gebuhr, and S. Anders. Macroscopic model based on application of representative volume element for steel fiber reinforced high performance concrete. In A. Zingoni, editor, *Current Perspectives and New Directions in Mechanics, Modelling and Design of Structural Systems: Proceedings of the Eigth International Conference on Structural Engineering, Mechanics and Computation (SEMC 2022), Cape Town, South Africa*, pages 1300–1306. CRC Press, Oxon, United Kingdom, 2022.

M. Pise, D. Brands, and J. Schröder. Development and calibration of a phenomenological material model for steel fiber reinforced high performance concrete basedon unit cell calculations. *Materials*, submitted 2024.

K. Seleš, T. Lesičar, Z. Tonković, and J. Sorić. A residual control staggered solution scheme for the phase-field modeling of brittle fracture. *Engineering Fracture Mechanics*, 205: 370–386, 2019. ISSN 0013-7944. doi: 10.1016/j.engfracmech.2018.09.027.

J. Storm, M. Pise, D. Brands, J. Schröder, and M. Kaliske. A comparative study of micro-mechanical models for fiber pullout behavior of reinforced high performance concrete. *Engineering Fracture Mechanics*, 243:107506, 2021. 10.1016/j.engfracmech.2020.107506.

R. L. Taylor. FEAP - finite element analysis program, version 8.2, 2008. URL `http://www.ce.berkeley/feap`.